Effect of directional solidification on texture and magnetic-field-induced strain in Ni–Mn–Ga foams with coarse grains

Peiqi Zheng,[a] Nikole J. Kucza,[b] Zilong Wang,[a,c] Peter Müllner[b] and David C. Dunand[a,*]

[a]Department of Materials Science & Engineering, Northwestern University, Evanston, IL 60208, USA
[b]Department of Materials Science & Engineering, Boise State University, Boise, ID 83725, USA
[c]Department of Materials Science & Engineering, Beijing Institute of Technology, Beijing 100081, China

Abstract—Ferromagnetic Ni–Mn–Ga shape memory alloys with large magnetic-field-induced strains are promising candidates for actuators. Here, we cast replicated Ni–Mn–Ga foams with 57 vol.% of 355–500 μm open pores, with and without directional solidification. The 10M martensitic phase was determined in all foam samples. Directionally solidified foam had a fiber texture, with <1 0 0> closely aligned with the solidification direction. In contrast, foams without directional solidification were more randomly textured. One directionally solidified foam showed a maximum magnetic-field-induced strain of 0.65%, which was twice the value displayed by other foams without directional solidification. This improvement is consistent with a reduction in incompatibility stresses between neighboring grains deforming by twinning, generated by a reduction in crystallographic misorientation in textured foam.

1. Introduction

Adding porosity to polycrystalline Ni–Mn–Ga ferromagnetic shape memory alloys boosts their magnetic-field-induced strain (MFIS) by reducing incompatible stresses between neighboring grains that deform via twinning. A fully reversible MFIS of ∼0.12% was obtained in polycrystalline Ni–Mn–Ga foams with 76 vol.% open porosities by introducing 355–500 μm pores separated by struts with bamboo grains, a structure which reduces strain incompatibilities between grains [1]. A 2.0–8.7% MFIS was measured in a 62% porous polycrystalline Ni–Mn–Ga foam displaying two populations of pores – larger, 500–600 μm pores and smaller, 75–90 μm pores within the struts and nodes surrounding the larger pores – which further decreases the hindrances to twinning due to grain boundaries [2].

Introducing texture is another method to reduce the constraints imposed by grain boundaries and increase the MFIS in polycrystalline Ni–Mn–Ga bulk materials. However, polycrystalline Ni–Mn–Ga bulk alloy with preferred grain orientation was found to exhibit negligible MFIS [3,4]. The following reports illustrate that texture can nevertheless enhance the MFIS either in Ni–Mn–Ga alloys with a large number of grain boundaries after (magneto-)mechanical training or in polycrystalline Ni–Mn–Ga

alloys with a high surface area to volume ratio and a reduced number of grain boundaries. A magneto-mechanically trained polycrystalline Ni–Mn–Ga bulk alloy (with a twinning stress below the stress which is produced by a magnetic field due to magnetic anisotropy) exhibited 0.5% MFIS when it was subjected to compressive deformation with a superimposed magnetic field (0.7 T) the axis of which was perpendicular to the axis of the applied stress (2 MPa as the initial value), while the axis of the columnar grains was parallel to the load axis [5]. Directionally solidified polycrystalline Ni–Mn–Ga plates, with a thickness comparable to the grain diameter and columnar grains with a strong fiber texture, demonstrated a 0.16% fully resettable MFIS after being trained by alternately compressing along the length and thickness directions [6,7]. Seven pieces of melt-spun polycrystalline Ni–Mn–Ga ribbon (with a thickness and width of about 0.12 and 14 mm, respectively) were bonded by a cyanoacrylate adhesive in the thickness direction. The ribbon, which presented a columnar crystal texture along the thickness direction, displayed improved magnetocrytalline anisotropy, leading to a larger MFIS in that direction. At a magnetic field of 1 T, the bonded ribbons showed a contractive martensitic transformation strain of −0.46% upon cooling from 27 to −73 °C [8].

Directional solidification (DS) and plastic deformation are two main fabrication processes used to produce elongated grains with specific, strong textures in polycrystalline Ni–Mn–Ga materials, beneficial for obtaining enhanced

* Corresponding author; e-mail: dunand@northwestern.edu

MFIS [9,10]. Plastic deformation includes hot rolling [11], hot extrusion [12] or high-pressure torsion [13] at 1000 °C when Ni–Mn–Ga is in its ductile phase with a B2 structure. However, a large degree of cold deformation has to be accumulated prior to recrystallization to achieve a strong texture. A strong overall texture cannot be achieved due to Ni–Mn–Ga's brittleness at low temperature and its tendency for dynamic recrystallization [14,15]. As compared to previous DS studies of bulk Ni–Mn–Ga [4,5,9], the present study uses slower DS rates, which encourage the creation of elongated grains that are aligned well with the thermal flow direction, contributing to a larger MFIS. Also, to the best of our knowledge, no studies have been performed on textured polycrystalline Ni–Mn–Ga foams.

In this study, two Ni–Mn–Ga foams with coarse grains, one directionally solidified and the other non-directionally solidified, were fabricated by the cast replication method. Their microstructure, thermal properties and phase constituents are reported and compared to those of control dense samples created by the same method. The effect of texture introduced by DS on enhancing the MFIS of a coarse-grained Ni–Mn–Ga foam is investigated.

2. Experimental procedures

2.1. Foam preparation

Polycrystalline Ni–Mn–Ga foams with and without DS were created by the cast replication technique [1], illustrated schematically in Fig. 1. First, about 2.2 g of sodium aluminate powders (sieved to 355–500 μm size) were partially sintered in air at 1500 °C for 3 h within a small (9.7 mm diameter) alumina crucible (B in Fig. 1) to create a preform with open porosity. A vacuum-cast ingot (~24 g), with the nominal composition $Ni_{49.0\pm0.2}Mn_{29.6\pm0.2}Ga_{21.4\pm0.2}$ at.%, was placed on top of the preform within the small alumina crucible, which was placed within a large alumina tube (C in Fig. 1). The first thermocouple (T1 in Fig. 1) was

A. Vertical tube furnace; B. Small alumina crucible;
C. Large alumina crucible; T1. Thermocouple 1; T2. Thermocouple 2;
F. Unislide; G. Heating elements of the furnace;
H. Ni-Mn-Ga/NaAlO₂composite I or II. (not drawn to scale)

Fig. 1. Schematic illustration of the furnace used for casting replications of Ni–Mn–Ga foam with or without DS.

attached at the bottom of the alumina tube to track the initial solidification point of the melt, which was taken as ~1100 °C, the solidus temperature of Ni–Mn–Ga [16]. A near-constant thermal gradient of ~2.7 °C mm^{-1} was measured in the furnace between 1000 and 1200 °C. Before solidification, the bottom end of each ingot was positioned close to the middle of the furnace, where a second thermocouple (T2 in Fig. 1) was positioned to measure the highest temperature of the furnace. The tube was heated under a vacuum of 0.47mPa until the second thermocouple measured a temperature of 1200 ± 10 °C. After ~1 h at this temperature, high-purity argon gas was introduced into the large alumina crucible at an absolute pressure of 136 kPa (1.34 atm) to force the molten alloy into the space holder preform. The resulting Ni–Mn–Ga/NaAlO₂ composite (ingot N, with a height of 15 mm) was solidified non-directionally, with the crucible immobile while the furnace temperature was dropped from 1200 to 1050 °C in 4 min and from 1050 to 700 °C in 25 min.

Another Ni–Mn–Ga/NaAlO₂ composite (ingot D, with a height of ~15 mm) underwent the same processing steps as ingot N up to the stage where the second thermocouple read 1200 ± 10 °C for 1 h. Subsequently, while keeping the temperature measured by the first thermocouple constant, ingot D was directionally solidified by lowering the large alumina crucible in steps of 10 mm every minute, using a linear slide (F in Fig. 1), until the whole ingot passed the solidus line at ~1100 °C. The ingot was then furnace-cooled in a similar manner as ingot N.

Each ingot was cut with a diamond saw to create two parallelepiped specimens per ingot, with approximate dimensions of $2 \times 3 \times 6$ mm³. Most of the sodium aluminate space holder was removed from these specimens by sonicating in a solution of 34 mol.% deionized water for ~14 h. Further immersion in 10 mol.% HCl for ~30–40 h removed the remaining sodium aluminate and thinned the foam struts by dissolution. The resulting four foams were labeled N1 and N2, for the non-directionally solidified ingot N, and D1 and D2, for the directionally solidified ingot D. The average porosities of all foams, as determined by measurements of mass and volume, were 58 ± 2 vol.% for foams N1 and N2 and 57 ± 2 vol.% for foams D1 and D2. To achieve the L2₁-ordered structure, the four foams were sealed in a quartz capsule with Ti getters under ~50 torr residual pressure and subjected to a stepwise heat treatment (725 °C/2 h, 700 °C/10 h, 500 °C/20 h) followed by air cooling.

2.2. Magnetic properties and MFIS

The magnetic saturation (M_{sat}) of the foams was determined using a MicroSense Model 10 vibrating sample magnetometer (VSM). During VSM saturation experiments, an external electromagnetic field was applied to the mounted $2 \times 3 \times 6$ mm³ vibrating foams and their magnetization (M) was measured as a function of the applied magnetic field ($\mu_0 H$) from ~0 to 0.2 T with a 0.01 T step within 5 min, from 0.2 to 1.95 T with a 0.05 T step within 8.75 min and from 1.95 to 2 T with a 0.01 T step within 1.25 min. The composition (determined with energy-dispersive spectroscopy) and transformation temperatures (determined with VSM) of the foams are given in Table 1. The MFIS was determined using a dynamic magneto-mechanical testing (DMMT) device [2,17]. The elongation
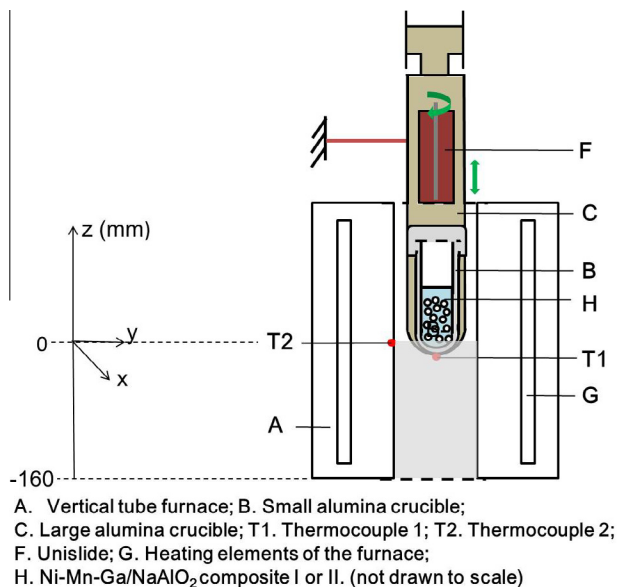
Table 1. Compositions and transformation temperatures of all foam samples.

| Foam	Composition (at.%)			Transformation temperature (°C)				
	Ni	Mn	Ga	M_s	M_f	A_s	A_f	T_c
N1	50.0 ± 0.2	28.7 ± 0.2	21.3 ± 0.1	54 ± 2	48 ± 1	55 ± 1	62 ± 2	98 ± 1
N2	50.1 ± 0.1	28.8 ± 0.3	21.1 ± 0.2	55 ± 1	41 ± 1	53 ± 1	63 ± 1	98 ± 2
D1	49.0 ± 0.0	30.1 ± 0.2	20.9 ± 0.2	48 ± 2	33 ± 1	43 ± 1	52 ± 2	102 ± 1
D2	49.0 ± 0.1	29.7 ± 0.1	21.3 ± 0.2	46 ± 2	33 ± 1	44 ± 1	52 ± 2	101 ± 1

was deflected through a mechanical lever and measured with an optical displacement sensor (Heidenhain MT 1281), with a displacement resolution better than 20 nm. The apparatus and the method of strain measurement are described in detail in Ref. [2]. Each $2 \times 3 \times 6$ mm^3 foam sample was mounted on its 2×3 mm^2 end faces, using a thin layer of superglue, onto the center of a sample holder on one side and onto a sliding head on the other side. The MFIS was measured along the longest axis of the sample, measuring ~6 mm. The mounted sample was then placed in the DMMT chamber, with a magnetic field of 0.97 T, perpendicular to the magnet rotation axis, provided by a Halbach cylinder. The MFIS was measured while the permanent magnet rotated at 30 rpm. The maximum and minimum extensions of the sample occurred when the magnetic field was perpendicular and parallel to the long axis of the sample, respectively; the difference between these values defined the MFIS. The MFIS was recorded for 20 revolutions, with 500 data points per revolution, while the temperature was increased or decreased. Thus, the temperature varied slightly for each measurement [2]. Approximately 100 revolutions were recorded at room temperature before the temperature of the sample was decreased by blowing laboratory air, chilled in copper tubing via a bath of liquid nitrogen, into the sample chamber until the temperature reached approximately 10 °C. The air was then routed through a copper coil, heated with an industrial heat gun, until the temperature reached approximately 50 °C. The sample was then cooled again with chilled air to approximately 10 °C. During this cooling step, the chilled air escapes in bursts, due to high pressure in the copper line, resulting in a fast cooling rate that was difficult to regulate.

2.3. X-ray diffraction

The martensite structure was determined using a Bruker AXS D8 Discover X-ray diffractometer (XRD) with a Cu K_a source and an area detector. The angle of the incident beam and the angle of the center position of the area detector were simultaneously increased in increments of 5° so that the 2θ angle covered the range from 40 to 90°. Measurements were completed on all six surfaces. While the diffracted intensity was recorded for 30 s, the sample stage was moved in the X and Y directions (Fig. 2) such that the beam covered the entire sample. Furthermore, the table rotated to cover the full Φ range.

To characterize texture, pole figures were measured on the face with edges of approximately 2×3 mm^2, which was perpendicular to the solidification direction for the directionally solidified samples.

Synchrotron high-energy X-ray diffraction (0.111538 Å in wavelength) experiments were conducted at beamline 11-ID-C, Advanced Photon Source (APS), Argonne
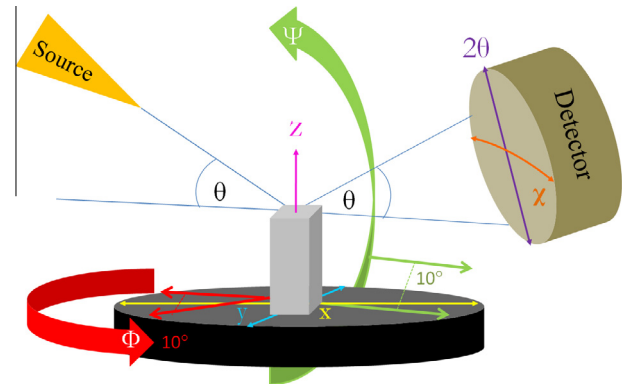

Fig. 2. XRD stage geometry in relation to the sample. Measurements were performed in 10° increments of Ψ, from 0 to 90°, and Φ, from 0 to 360°, to reveal texture and grain information.

National Laboratory. Two sample bars, with dimensions of $6.3 \times 2.5 \times 2.3$ mm^3 and $5.6 \times 2.9 \times 1.9$ mm^3, were cut respectively from the directionally solidified and as-cast foams. A sample stage with a three-axis goniometer was used to rotate and tilt to find the particular relationship between the sample and the incident beam. The sample was rotated along the vertical axis over a range from -5 to $+5°$ to allow a wider coverage of reciprocal space. A two-dimensional (2-D) area detector was used to collect the diffraction spots. The X-ray beam was focused to 0.5×0.5 mm^2. For each sample, six patterns were recorded equidistant along the length of the sample. Additionally, for a particular position, the sample was oriented with $<001>$ parallel to the beam and rocked by $\pm 5°$ to produce a 001 diffraction pattern.

2.4. Composition, microstructure and thermal characterization

The chemical composition of each of the four foam specimens was averaged from three areas (with approximate size 400×300 μm^2), located near the top, middle and bottom cross-section regions, via scanning electron microscopy (Hitachi S-3400N) with an energy-dispersive spectroscope (Oxford). The measurements were all collected using the same instrument parameters (i.e. accelerating voltage, probe current, working distance) and calibrated with an Ni–Mn–Ga standard sample the chemical composition of which was measured independently by wet chemical analysis.

Additional samples from the two ingots were cut for metallographic observation. The mounted and polished samples were etched with the Kalling II microetchant (40–80 ml ethanol + 40 ml HCl + 2 g CuCl$_2$) for a few minutes, heated to ~90 °C in air for 10 min and quenched
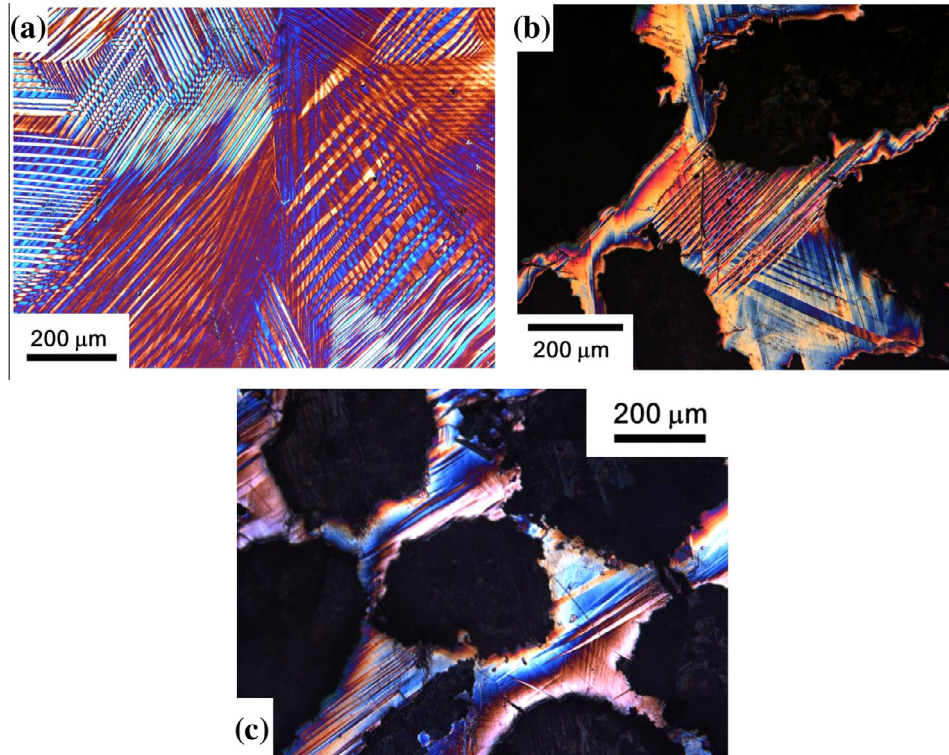
Fig. 3. Optical micrograph using cross-polarized filters of etched polished cross-sections of: (a) the bulk region of non-directionally solidified ingot N; (b) the porous region of ingot N; and (c) the porous region of directionally solidified ingot D.

in ice water. The samples were then imaged with an optical microscope (Olympus) under polarized light.

The transformation temperatures – martensite start and finish temperatures (M_s and M_f), austenite start and finish temperatures (A_s and A_f), and Curie temperature (T_c) – were determined using a MicroSense Model 10 VSM. During VSM temperature experiments, the $2 \times 3 \times 6$ mm^3 parallelepiped specimens were cooled from room temperature to -30 °C, at which point an external magnetic field of 0.025 T was applied and measurements were collected every 0.5 ± 0.1 °C at a heating rate of 6 °C min^{-1} from -30 to 150 °C and at a cooling rate of 4 °C min^{-1} from 150 to -30 °C to produce a plot of magnetization vs. temperature.

3. Results and discussion

3.1. Composition, microstructure and thermal properties

Table 1 lists the compositions of the four foams. All Ni–Mn–Ga foam specimens fall into the single β-Ni$_2$MnGa phase area, in the range of composition displaying a magnetic shape memory effect [18].

Martensite twins were found in the cross-sections of both specimens cut from ingot N, from the non-porous region above the foam and from the foam region, as shown in Fig. 3. In Fig. 3a, the grain boundaries for the bulk sample are not identified, and it appears that the grain size is on the order of millimeters, based on the interconnected martensitic twins in this cross-section. This microstructure is very similar to the reported microstructures of bulk MSMA studied with electron backscatter diffraction [19,20]. Fig. 3b and c show that Ni–Mn–Ga foams have different microstructures without and with DS at the same magnification.

It is difficult to unequivocally identify large grains due to the presence of pores, but twins span the full width of struts, indicating that the struts have a bamboo-like microstructure or are even monocrystalline. For the directionally solidified foam, as shown in Fig. 3c, most of the martensite variants are oriented in the same direction, which is consistent with the presence of a strong texture introduced by DS. As a comparison, there are three martensite variants with different orientations in the foam without DS (Fig. 3b), which is consistent with a more random distribution of grain orientations.

The transformation temperatures measured by VSM are summarized in Table 1. The martensite finish temperatures are above room temperature, which is in agreement with the martensitic structure (Fig. 3) and the X-ray diffraction results, revealing single phase 10M martensite (Fig. 4). The M_f values for specimens D1 and D2 are lower than those for specimens N1 and N2, and closer to ambient temperature.

3.2. MFIS measurement

The MFIS of the polycrystalline directionally solidified foam D1 was 0.65%, more than twice that of foam N1 (0.25%), which was without DS (Fig. 5). These MFIS values are an order of magnitude higher than that of a polycrystalline bulk Ni–Mn–Ga sample with DS, which was reported by Guo et al. [4] to be 0.06%. This small MFIS measured using a strain gauge under a magnetic field of >0.5 T in polycrystalline Ni–Mn–Ga bulk samples with an oriented grain structure (estimated from micrographs to be ~250 µm in the shortest direction and approaching 1 mm in the elongated direction) prepared by DS was twice as large as that for an as-cast sample with the same compo-
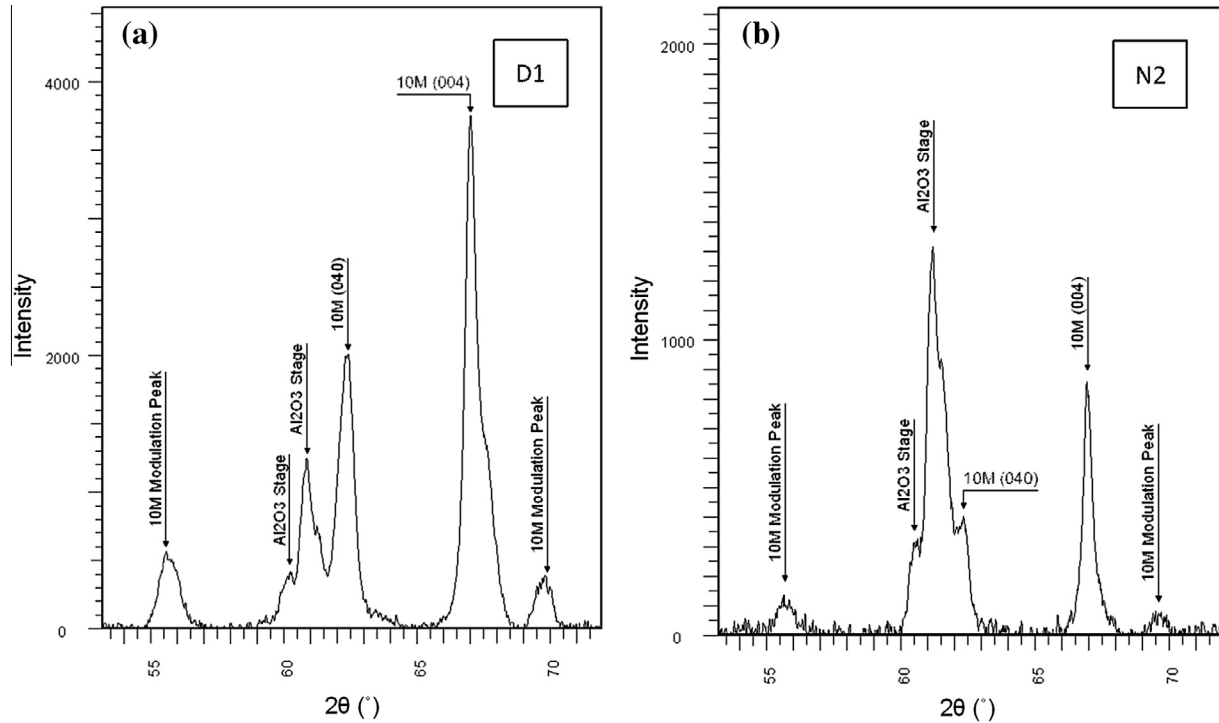
Fig. 4. XRD spectra (scanning over 2θ) of all six surfaces showing a 10M structure for (a) D1 and (b) N2 foams.

sition but randomly distributed equiaxed grains with a grain size of about 300 μm.

The first temperature cycle exhibited a different strain profile than successive cycles, in both directionally (D1) and non-directionally solidified (N1) samples, which may be attributed to the initial application of an external field and a temperature gradient which in combination are likely to create a thermo-mechanical training effect which increased the MFIS [2]. Heating and cooling through the phase transformation changed the temperature at which the maximum strain occurred. This can be attributed to the rates of heating and cooling. The heating rate was better controlled than the cooling rate. However, neither rate was constant due to the manual operation. Fast temperature changes may lead to a temperature lag and cause an apparent temperature shift in the recorded temperatures. The thermocouple placed on the surface of the sample measured the temperature of a specific region that was similar in size to a grain. Therefore, the temperature associated with the maximum MFIS reflects the local temperature, and is affected by heating/cooling rates and the thermal contact of the thermocouple. However, the DMMT measures the global MFIS. Also, the martensitic transformation temperatures obtained by the VSM are global temperatures. Therefore, the discrepancy that the temperature of maximum strain is below the martensitic finish temperature may reflect a difference between local and global temperature measurements of the sample.

3.3. Phase and texture characterization

Fig. 4 shows the X-ray spectra for (a) D1 and (b) N2 for the 2θ range between 51 and 74°. All reflections can be assigned to the 10M martensite structure or to Al_2O_3, which stemmed from the sample holder, indicating that both samples were single phase 10M martensite at room temperature. The 10M reflections are indexed according to the pseudo-tetragonal unit cell. The intensities of the (040) and (004) reflections were about four times stronger for the directionally solidified sample than for the non-directionally solidified sample (in absolute units and also in comparison with the Al_2O_3 reflections, which may serve as an internal standard). The higher intensity of the (040)/(004) reflections of D1 compared to N2 indicates a preferential orientation of grains with <100> closely parallel to the solidification direction.

Fig. 6 shows two (004) pole figures, for samples D1 (Fig. 6a) and N2 (Fig. 6b), respectively. Both pole figures show a single strong peak with non-centro-symmetric discoloration, indicating a single grain with multiple twinned martensite variants. For D1, the center of the peak was approximately 10° off the center of the pole figure. Thus, during solidification, the <100> direction was about 10° off the solidification direction. This orientation compares to the preferred orientation grains in directionally solidified bulk samples [7]. For N2, the center of the peak was approximately 20° off the center of the pole figure. For the directionally solidified sample, the six diffraction patterns collected at the synchrotron source along the length direction of the foam were identical in spot positions, indicating that the sample contains a very long grain and potentially is a single crystal. In contrast, the patterns collected along the length axis of the as-cast foam change with different positions, indicating that the sample consisted of several grains. The (001) diffraction patterns for both samples are shown in Fig. 7, clearly demonstrating the superlattice reflections of the 10M structure. The diffraction pattern
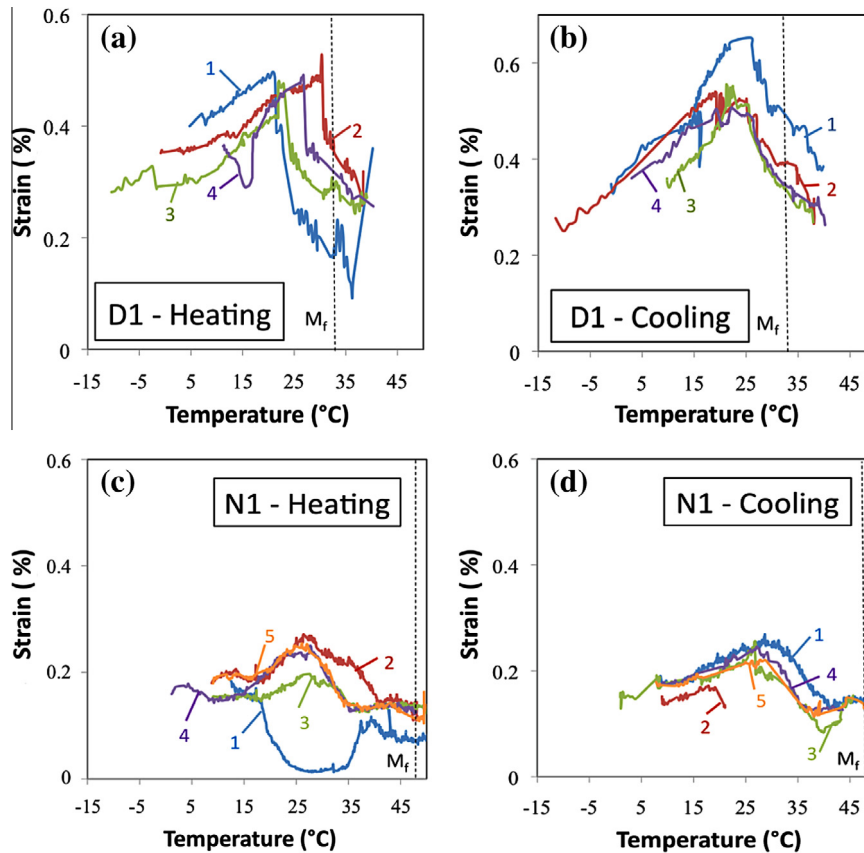
Fig. 5. Plot of MFIS vs. temperature for foam D1 showing (a) the heating portions of four consecutive cycles and (b) the corresponding cooling portions. Corresponding plots for foam N1 showing (c) the heating portions of five consecutive cycles and (d) the corresponding cooling portions.
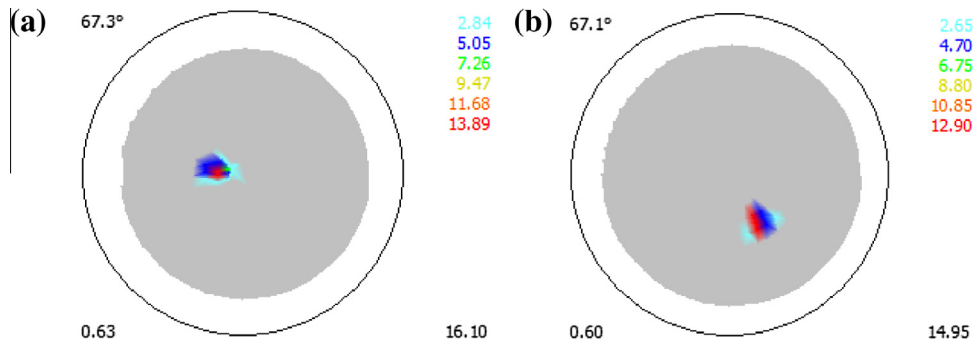
Fig. 6. Pole figures recorded with the (004) reflection for samples (a) D1 and (b) N2. Both pole figures show a strong peak, indicating a predominant large grain with multiple twinned martensite variants.

of D1 (Fig. 7a) shows a single grain with three twinned martensite variants, M1, M2 and M3 (all indexed based on the 10M modulation structure [21]). The diffraction pattern of N2 (Fig. 7b) shows two grains.

These results reflect a strong fiber texture for the directionally solidified sample with the <1 0 0> direction inclined by 10° to the solidification direction. While only one strongly elongated grain was detected with the synchrotron experiments, it is possible that the directionally solidified samples contain several long grains extending throughout the entire length of the samples. This result is in good agreement with the <1 0 0> fiber texture of directionally solidified bulk alloys, for which the deviation of <1 0 0> from the solidification direction was less than 10° and the grains of which were several millimeters long [6]. In comparison,

the non-directionally solidified <1 0 0> direction was more randomly oriented and the grains were smaller.

3.4. Texture and MFIS

Grain boundaries impose constraints to twinning and obstruct twinning effectively in Ni–Mn–Ga magnetic shape memory alloys. Pores reduce these constraints and increase the MFIS in polycrystalline Ni–Mn–Ga compared to similar non-porous bulk alloys [1]. In a randomly textured foam, the constraints imposed by grain boundaries can be further reduced via the introduction of small pores in large struts, resulting in a large increase in the MFIS [2]. Here, we reduced the grain boundary constraints via texture. The misorientation between neighboring grains in a
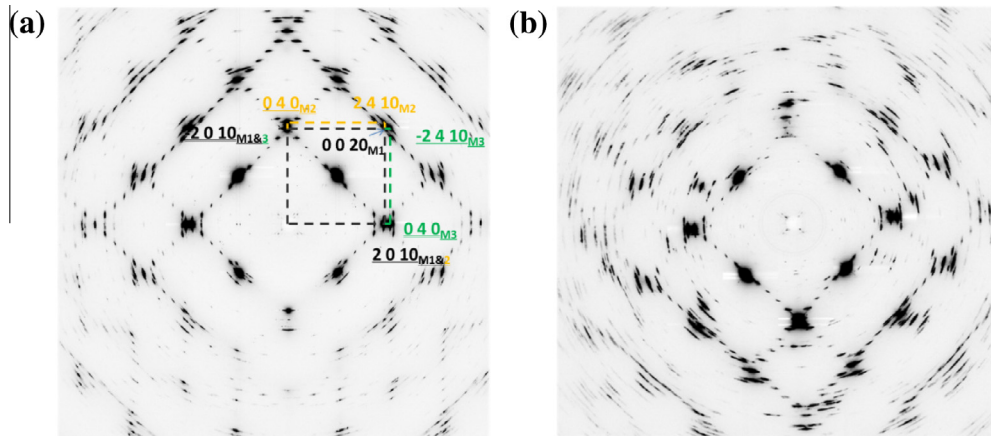
Fig. 7. <0 0 1> diffraction patterns for (a) D1 and (b) N2. There are three twinned martensite variants (M1, M2 and M3) present in D1. The pattern for N2 shows two different grains.

textured polycrystalline alloy is less than in randomly textured grains. In foam, where neighboring struts have different crystallographic orientations, less misorientation translates into a reduction of constraints for deformation because less hinging is required to accommodate the differences in deformation. A reduction of constraints allows for more twinning, and thus a higher MFIS, in more strongly textured foam than in less textured or untextured foam.

4. Conclusions

Ferromagnetic shape memory Ni–Mn–Ga foams with 57 ± 3 vol.% open pores (355–500 μm in size) were fabricated by the casting replication method with and without directional solidification (DS). DS resulted in foams with preferred orientation of grains with <1 0 0> around 10° to the solidification direction inside the directionally solidified foam. The foam without DS exhibited more randomly orientated grains. Both directionally solidified and non-directionally solidified samples exhibited an oligocrystalline microstructure with a 10M martensite structure at room temperature. The maximum MFIS of a directionally solidified foam was ~0.65%, which is more than twice as high as that of a foam specimen without DS (~0.25%). The increased MFIS in directionally solidified foam results from a texture-induced reduction of grain boundary constraints, which causes an increase in twin boundary mobility.

References

[1] Y. Boonyongmaneerat, M. Chmielus, D.C. Dunand, P. Müllner, Phys. Rev. Lett. (2007) 99.
[2] M. Chmielus, X.X. Zhang, C. Witherspoon, D.C. Dunand, P. Müllner, Nat. Mater. 8 (2009) 863.
[3] U. Gaitzsch, M. Potschke, S. Roth, B. Rellinghaus, L. Schultz, Acta Mater. 57 (2009) 365.
[4] S.H. Guo, Y.H. Zhang, Z.Q. Zhao, J.L. Li, X.L. Wang, Acta Phys. Sin-Ch. Ed. 53 (2004) 1599.
[5] S. Roth, U. Gaitzsch, M. Potschke, L. Schultz, Adv. Mat. Res. 52 (2008) 29.
[6] M. Potschke, S. Weiss, U. Gaitzsch, D.Y. Cong, C. Hurrich, S. Roth, L. Schultz, Scripta Mater. 63 (2010) 383.
[7] M. Potschke, S. Roth, U. Gaitzsch, C. Hurrich, A. Bohm, L. Schultz, Mater. Sci. Forum 684 (2011) 129.
[8] S.H. Guo, Y.H. Zhang, J.L. Li, Y. Qi, B.Y. Quan, X.L. Wang, Chin. Phys. Lett. 23 (2006) 227.
[9] R. Chulist, M. Poetschke, A. Boehm, H.-G. Brokmeier, T.L. Ulf Garbe, C-G. Oertel, W. Skrotzki, MRS Proc. (2007) 1050.
[10] U. Gaitzsch, J. Romberg, M. Pötschke, S. Roth, P. Müllner, Scripta Mater. 65 (2011) 679.
[11] A. Bohm, S. Roth, U. Gaitzsch, R. Chulist, W. Skrotzki, H. Kunze, W.G. Drossel, R. Neugebauer, Actuator 23 (2008) 742.
[12] R. Chulist, A. Bohm, T. Lippmann, W. Skrotzki, W.G. Drossel, R. Neugebauer, Ferromagnetic Shape Memory Alloys II 635 (2010) 195.
[13] R. Chulist, W. Skrotzki, C.-G. Oertel, A. Böhm, T. Lippmann, E. Rybacki, Scripta Mater. 62 (2010) 650.
[14] R. Chulist, Structure and properties of twin boundaries in Ni–Mn–Ga alloys (Ph.D thesis), Technischen Universität Dresden, 2011.
[15] U. Gaitzsch, R. Chulist, L. Weisheit, A. Bohm, W. Skrotzki, C.G. Oertel, H.G. Brokmeier, T. Lippmann, I. Navarro, M. Potschke, J. Romberg, C. Hurrich, S. Roth, L. Schultz, Adv. Eng. Mater. 14 (2012) 636.
[16] D.L. Schlagel, Y.L. Wu, W. Zhang, T.A. Lograsso, J. Alloys Compd. 312 (2000) 77.
[17] P. Müllner, V.A. Chernenko, G. Kostorz, J. Appl. Phys. 95 (2004) 1531.
[18] C. Wedel, K. Itagaki, J. Phase Equilib. 22 (2001) 324.
[19] D.Y. Cong, Y.D. Zhang, C. Esling, Y.D. Wang, X. Zhao, L. Zuo, J. Appl. Cryst. 44 (2011) 1033.
[20] Z. Li, X. Zhao, L. Zuo, C. Esling, Y. Zhang, Acta Mater. 59 (2011) 3390.
[21] G. Mogylnyy, I. Glavatskyy, N. Glavatska, O. Söderberg, Y. Ge, V.K. Lindroos, Scripta Mater. 48 (2003) 1427.